

First Detection of [C I] $^3\text{P}_1\text{--}^3\text{P}_0$ Emission from a Protoplanetary Disk

Takashi TSUKAGOSHI¹ Munetake MOMOSE¹ Masao SAITO² Yoshimi KITAMURA³
Yoshito SHIMAJIRI⁴ and Ryohei KAWABE⁵

ABSTRACT

We performed single point [C I] $^3\text{P}_1\text{--}^3\text{P}_0$ and CO $J=4\text{--}3$ observations toward three T Tauri stars, DM Tau, LkCa 15, and TW Hya, using the Atacama Large Millimeter/submillimeter Array (ALMA) Band 8 qualification model receiver installed on the Atacama Submillimeter Telescope Experiment (ASTE). Two protostars in the Taurus L1551 region, L1551 IRS 5 and HL Tau, were also observed. We successfully detected [C I] emission from the protoplanetary disk around DM Tau as well as the protostellar targets. The spectral profile of the [C I] emission from the protoplanetary disk is marginally single-peaked, suggesting that atomic carbon (C) extends toward the outermost disk. The detected [C I] emission is optically thin and the column densities of C are estimated to be $\lesssim 10^{16} \text{ cm}^{-2}$ and $\sim 10^{17} \text{ cm}^{-2}$ for the T Tauri star targets and the protostars, respectively. We found a clear difference in the total mass ratio of C to dust, $M(\text{C})/M(\text{dust})$, between the T Tauri stars and protostellar targets; the $M(\text{C})/M(\text{dust})$ ratio of the T Tauri stars is one order of magnitude smaller than that of the protostars. The decrease of the estimated $M(\text{C})/M(\text{dust})$ ratios for the disk sources is consistent with a theoretical prediction that the atomic C can survive only in the near surface layer of the disk and $\text{C}^+/\text{C}/\text{CO}$ transition occurs deeper into the disk midplane.

¹College of Science, Ibaraki University, Bunkyo 2-1-1, Mito 310-8512, Japan: ttsuka@mx.ibaraki.ac.jp

²Nobeyama Radio Observatory, Minamimaki, Minamisaku, Nagano 384-1305, Japan

³Institute of Space and Astronautical Science, Japan Aerospace Exploration Agency, Yoshinodai 3-1-1, Sagami-hara, Kanagawa 229-8510, Japan

⁴Laboratoire AIM, CEA/DSM-CNRS-Université Paris, Diderot, IRFU/Service d'Astrophysique, CEA, Saclay, F-91191 Gif-sur-Yvette Cedex, France

⁵National Astronomical Observatory of Japan, Osawa 2-21-1, Mitaka, Tokyo 181-8588, Japan

Subject headings: circumstellar matter — protoplanetary disks — stars: pre-main sequence — submillimeter: stars

1. Introduction

The gaseous component of protoplanetary disks is crucial for understanding the planet formation process because it affects the structures and evolution of the disk via chemical reactions. Theoretical studies have predicted that protoplanetary disks have multiple layers in their vertical direction due to stellar radiation. These include a relatively cool midplane, in which most of the molecules are depleted onto grains, a molecular-rich intermediate layer, and a hot surface layer (e.g., Bergin et al. 2007). Because the physical environment differs among layers, gas phase abundances also vary significantly.

Atomic carbon (C) is considered to be abundant in the disk surface where far-ultraviolet (FUV) photons drive the energy balance and gas chemistry, i.e., the photon dominated region (PDR). Theoretical studies predict that in the PDR, FUV photons with energies less than the ionization energy of hydrogen (13.6 eV) dissociate molecular hydrogen and carbon monoxide (CO) and ionize C to yield ionized carbon (C⁺) (Tielens & Hollenbach 1985). When significant attenuation is achieved, a thin H/H₂ transition layer should appear, beyond which hydrogen molecules dominate. Because the ionization energy of C is 11.6 eV, C⁺ is dominant at the lower density regions of the PDR. Deeper to the PDR, the carbon-ionizing radiation is attenuated, and CO forms via various chemical reactions. As a result, for the uniform PDR, C exists in a thin layer sandwiched between the C⁺ and CO layers.

Because photoevaporation at the disk surface is believed to govern the gas dispersal (Hollenbach et al. 1994, 2000), observations of C are crucial for understanding disk dissipation. Moreover, the observations of C are also important in terms of dust evolution in the disk because it affects the chemistry as a result of changes in the UV radiation field propagation and thus the intensity of the C line (Jonkheid et al. 2004).

However, detection of the submillimeter fine structure C lines has not been reported for protoplanetary disks thus far. Although a few studies have attempted to detect the emission lines of C from protoplanetary disks around intermediate-mass stars, only upper limits have been obtained (Chapillon et al. 2010; Panić et al. 2010; Casassus et al. 2013).

In this paper, we present the results of [C I] $^3P_1-^3P_0$ and $^{12}\text{CO } J=4-3$ observations with the Band 8 qualification model receiver mounted on the Atacama Submillimeter Telescope

Experiment (ASTE)¹, and report the first detection of [C I] emission from a protoplanetary disk. We estimate the optical depth of the emission to derive the column density of C, and discuss possible evolutionary trends in the total mass of atomic C.

2. Observations

We performed [C I] $^3\text{P}_1\text{--}^3\text{P}_0$ (492.161 GHz) and CO $J=4\text{--}3$ (461.041 GHz) observations toward three classical T Tauri stars (TTs), DM Tau, LkCa 15, and TW Hya, in November 2010 using the ASTE. Target information is listed in Table 1. In addition, we made [C I] observations toward two protostars (PSs) in Taurus, L1551 IRS 5 and HL Tau, to check the consistency of the observational data. We also used these data as a reference of the [C I] intensity during the PS phase of star formation.

The observations were taken with an ALMA Band 8 (400–500 GHz) qualification model heterodyne receiver (Band 8 QM; Satou et al. 2008) mounted on the ASTE. The Band 8 QM uses sideband separating receivers that detect two orthogonal polarizations and down-convert the sideband-separated intermediate frequency signals to 4–8 GHz. The half power beam width (HPBW) was $17''$ and the main beam efficiency η_{MB} was estimated to be 45% from observations of Jupiter. For the backend, we used MAC, a 1024 channel digital auto-correlator, which has a band width of 128 MHz and a resolution of 125 kHz, corresponding to 78 and 0.076 km s^{-1} , respectively.

The position switch method was employed and a single spectrum toward the source position was obtained for each target. Because our TTs targets are well known to be less affected by surrounding clouds, we selected OFF positions near the targets to effectively remove atmospheric fluctuations; 28, 15, and 1 arcmin from the stellar positions of DM Tau, LkCa 15, and TW Hya, respectively. For the PSs, we employed an OFF position of $(\alpha_{\text{J2000}}, \delta_{\text{J2000}}) = (4^{\text{h}} 32^{\text{m}} 6^{\text{s}}.0, 17^{\circ} 48' 51''.0)$, which was determined to avoid the CO $J=1\text{--}0$ emission of the L1551 cloud (Yoshida et al. 2010).

The telescope pointing calibration was performed every 1.5–2 hours by observing O-Cet and IRC+10216 in the CO $J=4\text{--}3$ emission line, and the resulting pointing accuracy was $\lesssim 3''$. Any time variation in intensity scale was checked by observing part of the Orion Horsehead nebula (position A; Philipp et al. 2006) two or three times daily and was found to be

¹The 10 m submillimeter telescope operated by Nobeyama Radio Observatory (NRO), a branch of National Astronomical Observatory of Japan, in collaboration with the University of Chile, and Japanese institutes including University of Tokyo, Nagoya University, Osaka Prefecture University, Ibaraki University, and Hokkaido University.

less than $\pm 10\%$. The [C I] data were obtained under good sky conditions ($\tau_{220\text{GHz}} \lesssim 0.05$), whereas $\tau_{220\text{GHz}} = 0.06\text{--}0.10$ for the CO observations. The single sideband system noise temperatures were typically 2100 K and 3100 K for [C I] and CO, respectively.

Data reduction and analysis were performed using the Common Astronomy Software Applications (CASA) version 3.3.0 software suite, in addition to its ASAP² modules. It should be noted that we reduced only one polarization dataset because of a beam alignment problem during the observations. Bad data were removed by the *sdf* task, baseline fitting and subtraction of the baseline from the spectra were performed with the *sdbaseline* task, and the data sets were combined in each source with the *sdaverage* task. The final spectra were obtained after smoothing with a five pixel boxcar function along the channel axis by the *sds* task, corresponding to a velocity resolution of $\sim 0.4 \text{ km s}^{-1}$.

3. Results

3.1. [C I] $^3\text{P}_1\text{--}^3\text{P}_0$ and CO $J=4\text{--}3$ spectra

Figure 1 shows the [C I] $^3\text{P}_1\text{--}^3\text{P}_0$ and CO $J=4\text{--}3$ spectra toward the three T Tauri star targets, and the derived spectral line parameters are listed in Table 2. We successfully detected [C I] emission with a peak intensity of $T_{\text{A}}^* = 0.12 \text{ K}$ toward DM Tau. The line profile is single peaked with a central velocity of $V_{\text{LSR}} = 6.1 \text{ km s}^{-1}$, which is consistent with the systemic velocity of the circumstellar disk as estimated by molecular line observations (5.9 km s^{-1} ; e.g., Handa et al. 1995). The emission appeared to be slightly asymmetric with

²ATNF Spectral Analysis Package

Table 1. Target information

Source	R.A. (J2000)	Decl. (J2000)	d (pc)	SP. type	M_* (M_{\odot})	Age (Myr)	$M(\text{dust})$ ($10^{-4} M_{\odot}$)	$R_{\text{disk}}(\text{CO})$ (AU)	incl. ($^{\circ}$)	f_{disk}	refs.
DM Tau	04:33:48.72	+18:10:10.0	140	M1	0.5	4.3	2.4	890	34	0.32	1,4,5,6
LkCa 15	04:39:17.80	+22:21:03.5	140	K5	1.0	3–12	4.8	905	52	0.25	1,6,7
TW Hya	11:01:51.91	−34:42:17.0	54	K7	0.8	10	3.4	215	7	0.15	2,8
L1551 IRS5	04:31:34.07	+18:08:04.9	140	5	1	1
HL Tau	04:31:38.44	+18:13:57.7	140	6	1	1,3

References. — (1) Andrews & Williams (2005); (2) Andrews et al. (2012); (3) Beckwith et al. (1990); (4) Kitamura et al. (2002); (5) Öberg et al. (2010); (6) Piétu et al. (2007); (7) Qi et al. (2003); (8) Wilner et al. (2000)

a somewhat larger extent to redshifted velocities. This is similar to the spectral shape of the CO $J=4-3$ and other CO transitions. (Guilloteau & Dutrey 1994; Thi et al. 2001). Here, the emission component visible near $\sim 9 \text{ km s}^{-1}$ was not analyzed because it most likely originates from the ambient cloud (Handa et al. 1995). For TW Hya and LkCa 15, we did not detect any [C I] emission, and obtained only the 3σ upper limits shown in Table 2. To estimate upper limits to the total integrated intensity of the [C I] emission lines, we assumed velocity widths of 3 and 1 km s^{-1} for LkCa 15 and TW Hya, respectively, the values obtained by single dish CO observations (van Zadelhoff et al. 2001).

Significant [C I] emission toward the PSs L1551 IRS 5 and HL Tau was detected, as shown in Figure 2. The spectral profiles are single-peaked at values close to their systemic velocities. The emission intensities are markedly higher than that of DM Tau.

Emission in the CO $J=4-3$ line was detected toward DM Tau and TW Hya. The peak velocities and line profiles are in good agreement with those of high- J CO spectra (Guilloteau & Dutrey 1994; Thi et al. 2001; van Zadelhoff et al. 2001). The double-peaked profile of DM Tau lies close to the systemic velocity. After correcting for the beam size and efficiency, the integrated intensity of CO emission from TW Hya was comparable to the marginal value reported by Kastner et al. (1997) within the uncertainties.

3.2. Optical depth of [C I] emission and C column density

We derived the optical depth of the [C I] emission and thus the C column density using the equations reported by Oka et al. (2001). The optical depth at the peak velocity, $\tau_{[\text{C I}]}$, is given by

$$\tau_{[\text{C I}]} = -\ln\left(1 - \frac{T_{\text{A}}^*/\eta_{\text{MB}}}{f_{\text{disk}}[J(T_{\text{ex}}) - J(T_{\text{bg}})]}\right), \quad (1)$$

where f_{disk} is the beam filling factor of the source, T_{ex} is the excitation temperature, T_{bg} is the temperature of the cosmic background radiation, and J is the radiation temperature defined by

$$J(T) = \frac{h\nu/k_{\text{B}}}{\exp(h\nu/k_{\text{B}}T) - 1}. \quad (2)$$

Here h is the Planck constant, ν is the observed frequency, and k_{B} is the Boltzmann constant. The factor f_{disk} was derived from the ratio of the solid angle of the disk to that of the telescope’s beam, $f_{\text{disk}} = \Omega_{\text{disk}}/\Omega_{\text{A}}$. The solid angle Ω_{disk} was estimated by assuming that the extent of the [C I] emission is identical to that of the resolved CO disk (Piétu et al. 2007; Andrews et al. 2012). The outer radius of the CO disk and its inclination angle, in addition to the estimated f_{disk} , are listed in Table 1. We employed $f_{\text{disk}} = 1$ for the PSs because

they were expected to be embedded in extended envelopes that extend over the beam area. For the TTSs, we assumed a constant T_{ex} of 50 K, as suggested by theoretical studies of protoplanetary disks around typical T Tauri stars that predict the $\text{C}^+/\text{C}/\text{CO}$ transition layer to appear at regions with $T_{\text{gas}} \sim 50$ K (Jonkheid et al. 2004; Kamp & Dullemond 2004). Conversely, we assumed $T_{\text{ex}} = 20$ K for the PSs, which is the accepted value for [C I] observations of a PS surrounded by an infalling envelope (Ceccarelli et al. 1998).

Assuming that local thermodynamic equilibrium (LTE) applies, we derived the averaged C column density over the source via

$$N(\text{C}) = 1.98 \times 10^{15} \frac{\int T_{\text{A}}^* dv}{\eta_{\text{MB}}} Q(T_{\text{ex}}) \exp\left(\frac{E_1}{kT_{\text{ex}}}\right) \times \left[1 - \frac{J(T_{\text{bg}})}{J(T_{\text{ex}})}\right]^{-1} \frac{\tau_{[\text{C I}]}}{1 - \exp(-\tau_{[\text{C I}]})} f_{\text{disk}}^{-1} . \quad (3)$$

Here, $Q(T_{\text{ex}})$ is the ground-state partition function for neutral atomic carbon,

$$Q(T_{\text{ex}}) = 1 + 3 \exp\left(-\frac{E_1}{kT_{\text{ex}}}\right) + 5 \exp\left(-\frac{E_2}{kT_{\text{ex}}}\right) , \quad (4)$$

where E_1 and E_2 are the energies of the $J = 1$ and 2 levels, respectively, and $\tau_{[\text{C I}]}$ is the velocity-averaged optical depth of the [C I] emission. In this study, however, we used the optical depth at the peak velocity instead of the velocity-averaged optical depth, which gives an upper limit to the column density. It should be noted that we assumed the optically thin condition ($\tau_{[\text{C I}]} \ll 1$) for LkCa 15 and TW Hya because no [C I] emission was detected. The C column density so estimated are listed in Table 3. The total mass of atomic carbon, $M(\text{C})$, was derived by integrating the column density over the solid angle of the source. Therefore, $M(\text{C})$ in the telescope beam can be uniquely determined regardless of source distribution.

Table 3 clearly shows that all the detected [C I] emission lines are optically thin. The estimated C column density of the TTSs is typically $\sim 10^{16} \text{ cm}^{-2}$ or less, whereas that of the PS is one order of magnitude higher ($\sim 10^{17} \text{ cm}^{-2}$). Accordingly, the $M(\text{C})$ values of the T Tauri star targets are one order of magnitude smaller than those of the PSs. These results can be attributed to the lack of dense envelopes around the TTSs.

4. Discussion

4.1. Origin of the [C I] emission

The [C I] emission detected from DM Tau is most likely associated with the rotating gas disk around the star. The peak velocity and full width half maximum are consistent with

those of the disk in molecular lines (e.g., Saito et al. 1995). Because of the modest upper energy of the ground state atomic C fine structure line (~ 24 K), the [C I] emission is likely to be weighted toward the emission from the outer most part of the disk due to beam dilution. In fact, the detected [C I] emission shows a single-peaked profile near the systemic velocity, suggesting that the emission may dominate at the region where the rotation velocity is small, i.e., the outer part of the disk if Keplerian rotation applies. In addition, the fact that the total mass of C is one order of magnitude smaller than those of the PSs (Table 3) supports the disk origin of the [C I] emission. However, the actual nature of the [C I] emission of DM Tau remains unclear due to the large HPBW of the telescope. High-resolution observations are required to reveal the detailed spatial distribution of the [C I] emission over the disk.

The estimated [C I] intensity of DM Tau is consistent with theoretical models of protoplanetary disk chemistry. Jonkheid et al. (2004), for example, calculated the [C I] line intensity of a T Tauri star with a massive disk of $0.07 M_{\odot}$ through a self-consistent treatment of the PDR near the disk surface. The resultant peak intensity is expected to be ~ 0.1 K in T_{A}^* after correcting for the ASTE beam size and the distance to the source, which is comparable to our observed intensity.

The higher intensities of the PSs than those of the TTSs suggest that the atomic carbon line originates mainly from the envelopes. Because the velocity width of the [C I] emission is much narrower than that of the wing emission of a molecular outflow ($\sim 10 \text{ km s}^{-1}$), the high velocity outflow is unlikely to affect the [C I] emission (Moriarty-Schieven et al. 2006; Stojimirović et al. 2006). There is a possibility of a low velocity cavity wall swept up by the outflow. High-resolution [C I] observations are required to separate the envelope from such a low velocity entrainment component.

4.2. Difference of $M(\text{C})/M(\text{dust})$ between T Tauri stars and protostars

We introduce the total mass ratio of atomic C to dust grains, $M(\text{C})/M(\text{dust})(\equiv R)$, to investigate the evolutionary variation of $M(\text{C})$. The dust mass, which is generally estimated by optically thin (sub-)millimeter continuum observations, reflects the total gas mass of the system if the gas-to-dust ratio is constant. Therefore, R is an indicator of a fraction of C with respect to the total amount of gas, which is described as $R \propto g/d \times X(\text{C})$, where g/d is the gas-to-dust ratio, and $X(\text{C})$ is the fractional abundance of C with respect to H_2 . It is important to state that, especially for a protoplanetary disk, the atomic C and the dust grains trace distinct vertical layers of the disk; the atomic C presumably exists in the disk near-surface layers while the dust grains are mainly at the disk midplane. Therefore, R practically indicates the mass of C near the PDR with respect to the total mass.

We compiled $M(\text{dust})$ from previous studies, as listed in Table 1. All $M(\text{dust})$ data, except that for TW Hya, were calculated from the total masses in Andrews & Williams (2005), who measured (sub-)millimeter flux densities with single dish telescopes. Their beam sizes were typically $\sim 10\text{--}15''$, which is comparable to that of our [C I] observations. These authors estimated the total (gas+dust) disk mass by a simple disk model with power-law density and temperature profiles under an assumed gas-to-dust ratio of 100. In Table 1, we show the dust mass after correcting for the assumed gas-to-dust ratio. For TW Hya, we took the mass estimate from Wilner et al. (2000), who also used a similar simple disk model to estimate the disk mass. Although their observations were made with an interferometer, the flux density of the entire disk was correctly recovered because the disk size is comparable to the detectable scale mentioned in Wilner et al. (2000).

The derived R is listed in Table 3. A clear difference in R is apparent between the TTSs and PSs; R is typically an order of 10^{-4} or less for the TTSs, whereas the PSs show $R = 3.4 \times 10^{-3}$, on average. It should be noted that these results are not significantly affected by the difference in the assumed value of T_{ex} . If we use $T_{\text{ex}} = 50$ K for the PSs, which is the same value as in the TTSs, we obtain $R = 2.7 \times 10^{-3}$, on average, a value still significantly higher than that for the TTS values. When $T_{\text{ex}} = 10$ K, a typical value in molecular cloud cores, the difference was more noticeable.

As defined above, the decrement of R can be interpreted by either a reduced $X(\text{C})$ or g/d . The former case means that $X(\text{C})$ decreases as star formation progresses. The chemical lifetime of C has been theoretically predicted to drop substantially with increments in the gas density (Leung et al. 1984). Because the gas density significantly increases from a tenuous protostellar envelope to a dense disk near a TTS, a reduction in $X(\text{C})$ is expected at the TTS stage. In fact, the typical density at the disk midplane is estimated to be $\sim 10^9 \text{ cm}^{-3}$ at 100 AU if we assume the minimum mass solar nebula (Hayashi 1981), whereas the typical density of the PSs is $\sim 10^5 \text{ cm}^{-3}$ (Momose et al. 1998; Saito et al. 2001). If the reduced g/d is the case, the gas in the disk must be depleted to a low level of $g/d \lesssim 10$ to explain the R decrement of at least one order of magnitude. However, such a high depletion of overall gas is not expected to occur in the disk, as discussed in §4.3.

4.3. Non detection of [C I] emission toward LkCa 15 and TW Hya

Only upper limits were obtained for the [C I] emission from LkCa 15 and TW Hya, despite the fact that they also have disks as massive as that of DM Tau. One possible explanation is that overall gas depletion with disk evolution leads to a depletion of C. Since all the targets are in the evolutionary stage of a so-called transitional disk, their disks are

expected to be evolved with respect to a filled disk (Andrews et al. 2011, 2012). Moreover, their advanced stellar ages imply that the disks of LkCa 15 and TW Hya are older than the DM Tau disk. The actual gas mass is difficult to directly estimate because of the large optical depths of molecular lines. Some modeling efforts by using CO data indicate a lower gas-to-dust ratio with respect to the standard interstellar value (Williams & Best 2014; Thi et al. 2010). However, as mentioned in §4.2, the gas mass estimation for TW Hya by an HD line emission, which is believed to be a good tracer of gas mass, indicates that the disk is massive so that the gas-to-dust ratio is comparable to the standard interstellar value (Bergin et al. 2013). Taking into account the fact that the disk model with a nominal gas-to-dust ratio of 100 reproduces well the observed intensity (Jonkheid et al. 2004), an overall gas depletion is unlikely the case. An alternative is the depletion of volatiles such as C-containing species at the surface with disk evolution. Such a time-dependent sink mechanism of C is proposed based on the observational data of HD and CO isotopologue lines (Favre et al. 2013).

We acknowledge the ASTE staff for the operation and maintenance of the observational instruments. We would like to thank H. Nomura and D. Ishimoto for fruitful discussions. T.T. and M.M. were supported by JSPS KAKENHI grant No. 23103004. Y.S. was supported by the French National Research Agency (grant No. ANR11BS560010 STARFICH).

Facilities: Atacama Submillimeter Telescope Experiment

REFERENCES

- Andrews, S. M., & Williams, J. P. 2005, *ApJ*, 631, 1134
- Andrews, S. M., Wilner, D. J., Espaillat, C., et al. 2011, *ApJ*, 732, 42
- Andrews, S. M., Wilner, D. J., Hughes, A. M., et al. 2012, *ApJ*, 744, 162
- Beckwith, S. V. W., Sargent, A. I., Chini, R. S., & Guesten, R. 1990, *AJ*, 99, 924
- Bergin, E. A., Aikawa, Y., Blake, G. A., & van Dishoeck, E. F. 2007, *Protostars and Planets V*, 751
- Bergin, E. A., Cleeves, L. I., Gorti, U., et al. 2013, *Nature*, 493, 644
- Casassus, S., Hales, A., de Gregorio, I., et al. 2013, *A&A*, 553, A64
- Ceccarelli, C., Caux, E., White, G. J., et al. 1998, *A&A*, 331, 372
- Chapillon, E., Parise, B., Guilloteau, S., Dutrey, A., & Wakelam, V. 2010, *A&A*, 520, A61

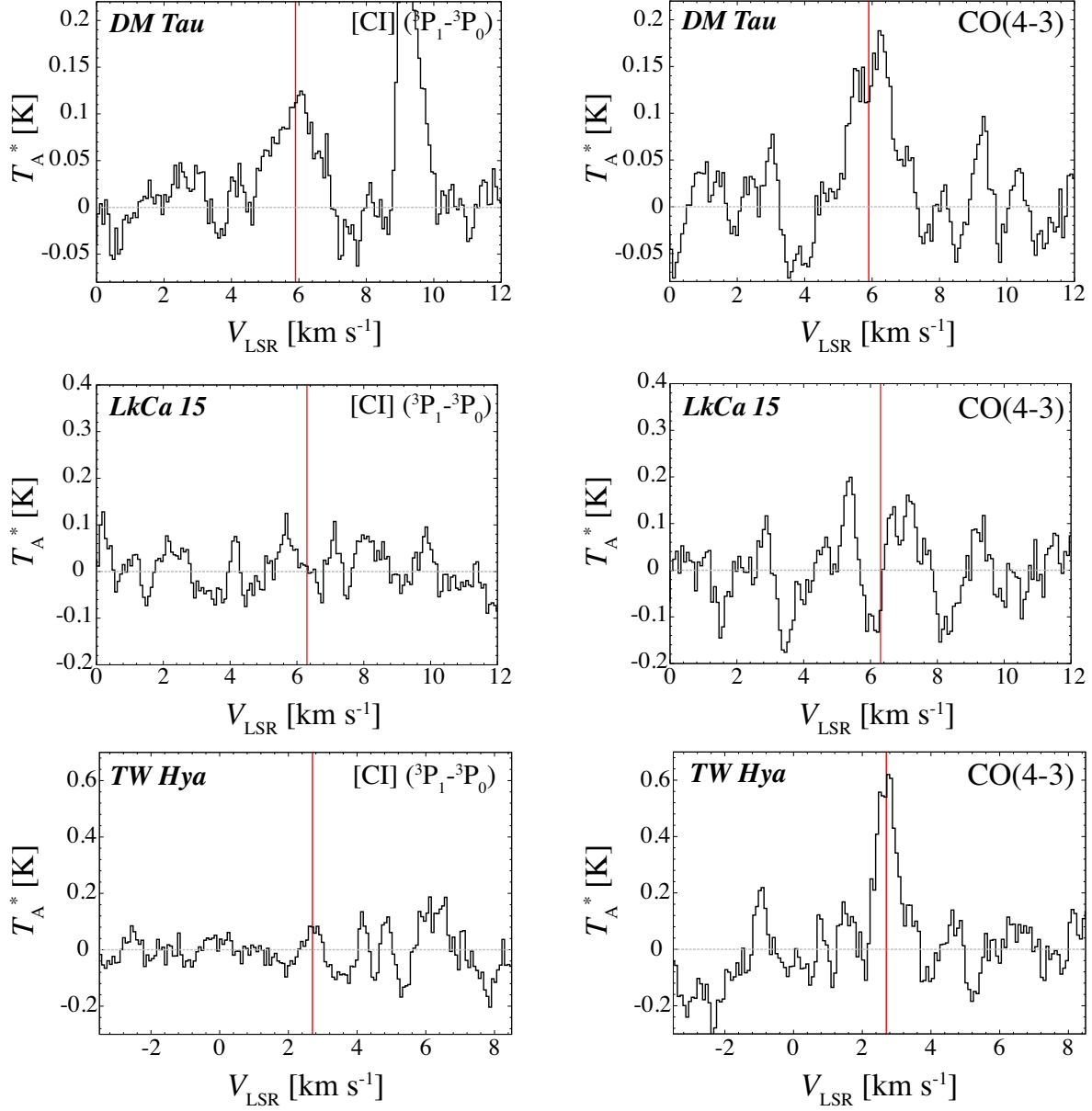


Fig. 1.— [C I] (left) and CO (right) spectra toward the three TTSs, DM Tau (top), LkCa 15 (middle), and TW Hya (bottom). The vertical red line indicates the systemic velocity of the circumstellar disk (Handa et al. 1995; Qi et al. 2003, 2004).

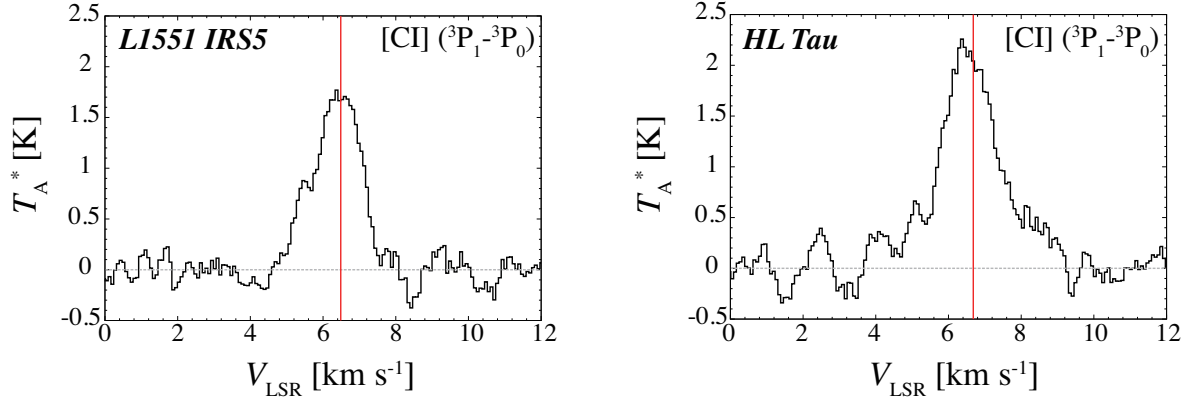


Fig. 2.— [C I] spectra of the PSs, L1551 IRS5 (left) and HL Tau (right). The vertical red lines indicate the systemic velocity (Saito et al. 2001).

Table 2. Parameters of [C I] $^3\text{P}_1\text{-}^3\text{P}_0$ and CO $J=4\text{-}3$ spectra

Source	[C I] $^3\text{P}_1\text{-}^3\text{P}_0$				CO $J=4\text{-}3$			
	T_A^{*1} (K)	V_{LSR} (km s^{-1})	ΔV (km s^{-1})	$\int T_A^* dv$ (K km s^{-1})	T_A^{*1} (K)	V_{LSR} (km s^{-1})	ΔV (km s^{-1})	$\int T_A^* dv$ (K km s^{-1})
DM Tau	0.12 ± 0.03	6.1	1.4	0.17 ± 0.05	0.18 ± 0.03	6.2	1.1	0.20 ± 0.05
LkCa 15	< 0.15	< 0.18
TW Hya	< 0.24	0.62 ± 0.08	2.8	0.7	0.43 ± 0.11
L1551 IRS 5	1.77 ± 0.10	6.3	1.6	2.77 ± 0.21
HL Tau	2.26 ± 0.08	6.4	2.0	4.55 ± 0.18

¹ 3σ upper limit for non-detection.

Note. — Column (1) gives the source name. Columns (2) and (6) give the peak intensity and root-mean-square noise level of the line in T_A^* . Columns (3) and (7) give the local standard-of-rest (LSR) velocity at the emission peak. Columns (4) and (8) give the velocity width in full width at half maximum (FWHM) of the line. Columns (5) and (9) give the total integrated intensity of the line and its uncertainty.

- Favre, C., Cleeves, L. I., Bergin, E. A., Qi, C., & Blake, G. A. 2013, *ApJ*, 776, LL38
- Fukagawa, M., Tsukagoshi, T., Momose, M., et al. 2013, *PASJ*, 65, L14
- Guilloteau, S., & Dutrey, A. 1994, *A&A*, 291, L23
- Handa, T., Miyama, S. M., Yamashita, T., et al. 1995, *ApJ*, 449, 894
- Hayashi, C. 1981, *Progress of Theoretical Physics Supplement*, 70, 35
- Hollenbach, D., Johnstone, D., Lizano, S., & Shu, F. 1994, *ApJ*, 428, 654
- Hollenbach, D. J., Yorke, H. W., & Johnstone, D. 2000, *Protostars and Planets IV*, 401
- Jonkheid, B., Faas, F. G. A., van Zadelhoff, G.-J., & van Dishoeck, E. F. 2004, *A&A*, 428, 511
- Kamp, I., & Dullemond, C. P. 2004, *ApJ*, 615, 991
- Kastner, J. H., Zuckerman, B., Weintraub, D. A., & Forveille, T. 1997, *Science*, 277, 67
- Kitamura, Y., Momose, M., Yokogawa, S., et al. 2002, *ApJ*, 581, 357
- Leung, C. M., Herbst, E., & Huebner, W. F. 1984, *ApJS*, 56, 231
- Maezawa, H., Ikeda, M., Ito, T., et al. 1999, *ApJ*, 524, L129
- Momose, M., Ohashi, N., Kawabe, R., Nakano, T., & Hayashi, M. 1998, *ApJ*, 504, 314
- Moriarty-Schieven, G. H., Johnstone, D., Bally, J., & Jenness, T. 2006, *ApJ*, 645, 357
- Öberg, K. I., Qi, C., Fogel, J. K. J., et al. 2010, *ApJ*, 720, 480
- Oka, T., Yamamoto, S., Iwata, M., et al. 2001, *ApJ*, 558, 176
- Panić, O., van Dishoeck, E. F., Hogerheijde, M. R., et al. 2010, *A&A*, 519, A110
- Philipp, S. D., Lis, D. C., Güsten, R., et al. 2006, *A&A*, 454, 213
- Piétu, V., Dutrey, A., & Guilloteau, S. 2007, *A&A*, 467, 163
- Qi, C., Kessler, J. E., Koerner, D. W., Sargent, A. I., & Blake, G. A. 2003, *ApJ*, 597, 986
- Qi, C., Ho, P. T. P., Wilner, D. J., et al. 2004, *ApJ*, 616, L11
- Saito, M., Kawabe, R., Ishiguro, M., et al. 1995, *ApJ*, 453, 384

- Saito, M., Kawabe, R., Kitamura, Y., & Sunada, K. 2001, *ApJ*, 547, 840
- Satou, N., Sekimoto, Y., Iizuka, Y., et al. 2008, *PASJ*, 60, 1199
- Stojimirović, I., Narayanan, G., Snell, R. L., & Bally, J. 2006, *ApJ*, 649, 280
- Suzuki, H., Yamamoto, S., Ohishi, M., et al. 1992, *ApJ*, 392, 551
- Thi, W. F., van Dishoeck, E. F., Blake, G. A., et al. 2001, *ApJ*, 561, 1074
- Thi, W.-F., Mathews, G., Ménard, F., et al. 2010, *A&A*, 518, LL125
- Tielens, A. G. G. M., & Hollenbach, D. 1985, *ApJ*, 291, 722
- van Zadelhoff, G.-J., van Dishoeck, E. F., Thi, W.-F., & Blake, G. A. 2001, *A&A*, 377, 566
- Williams, J. P., & Best, W. M. J. 2014, *ApJ*, 788, 59
- Wilner, D. J., Ho, P. T. P., Kastner, J. H., & Rodríguez, L. F. 2000, *ApJ*, 534, L101
- Yoshida, A., Kitamura, Y., Shimajiri, Y., & Kawabe, R. 2010, *ApJ*, 718, 1019

Table 3. Physical parameters derived from [C I] line.

Source	$\tau_{[\text{C I}]}$	$N(\text{C})$ (10^{16} cm^{-2})	$M(\text{C})$ ($10^{-7} M_{\odot}$)	$\frac{M(\text{C})}{M(\text{dust})}$ (10^{-4})
DM Tau	0.02	1.6 ± 0.5	0.75 ± 0.22	3.1
LkCa 15	<0.03	<4.1	<1.48	<3.1
TW Hya	<0.09	<3.6	<0.12	<0.4
L1551 IRS5	0.47	10.7 ± 0.8	15.3 ± 1.2	31
HL Tau	0.65	19.0 ± 0.8	27.4 ± 1.1	46

Note. — Column (1) gives the source name. Column (2) gives the optical depth of the [C I] line. Column (3) gives the column density of C after correction for the beam filling factor of the disk. Column (4) gives the total mass of C. Column (5) gives the ratio of the total mass of C to the dust mass listed in Table 1.